MULTI-RADAR DATA FUSION FOR HIGH-RESOLUTION QPE IN URBAN AREA

Brandon Hickman[1,2] Jussi Tiira[2] , Roberto Cremoni[2,3], Dmitri Moisseev[2,4]

[1] *University of Bonn, Germany*

[2] *Institute for Atmospheric and Earth System Research / Physics, University of Helsinki, Finland*

[3] *ARPA-Piemonte, Turin, Italy*

[4] *Finnish Meteorological Institute, Helsinki, Finland*

1. Introduction

Urban areas are at a high risk of extremes in precipitation where flooding can have large socio-economic impacts. High-quality observations are required in urban areas to allow adequate warnings and understanding of how precipitation affects the urban area. Weather radar, with their large large temporal and spatial coverage, are ideal instruments for precipitation observations (Saltikoff et al 2010). However, radars suffer from several challenges which are compounded for urban areas (Einfalt et al 2004; Berne et al 2004). Radar signal quality can be degraded due to several issues, including ground clutter, beam blockage, signal and radome attenuation and filtering techniques employed.

Figure 1:Helsinki area with three C band radars

The Helsinki region hosts three C band radars, the Vantaa radar (VAN) owned by the Finnish Meteorological Institute (FMI) and which is part of thee Finnish national radar grid, the Kumpula radar (KUM) maintained by the University of Helsinki, and the Kerava radar owned and operated by the Vaisala corporation, both of which are for research operations. The radars can be seen in Figure 1. Friedrich et al. (2006) used index fields to define the radar data quality. It is shown here, that by combining the three radars, after a series of quality control steps, into a single composite improves the possibility of quantitative precipitation estimation in urban areas. The sources of uncertainty we address here are 1) the removal of non-meteorological targets, 2) absolute calibration of radar reflectivity, 3) identification and correction of beam blockage, 4) ground clutter , 5) attenuation of the path and radome attenuation, 6) and beam broadening and precipitation overshooting.

2. Methods

2.1.Radar Composite and Quality Control

In order to produce the highest quality precipitation field for the urban area a three radar composite was created form the three Helsinki based radars: KER, KUM, and VAN. Prior to radar compositing the radar undergo a series of quality control steps to reduce the impact of various errors. These uncertainties are converted to a series of weights which are then applied to $Z_{H,}$ and K_{DP}. The weights for Z_H are as follows: non-meteorological targets (WNM), Beam Blockage (W_{BB}), path

attenuation (Watt), wet radome attenuation (W_{WR}), Doppler-filter clutter suppression (W_{vel}), ground clutter (W_{CSR}), and range (W_{range}). For K_{dp}, which suffers from fewer uncertainties than Z_H such as calibration, attenuation, and ground clutter, only the weights for range was used to correct for height differences in the beam. Additionally noise in light rain was accounted for by removing K_{dp}<0.1 ° km^{-1}. Additional filter, based on the self-consistency theory (Gorgucci et al 1992) was used to remove spurious results (W_{KDP}). The weights were combined as seen in (2.1) and the composite was created by the joining of the three quality controlled radars W_{KER}, W_{KUM}, W_{VAN} (2.2),

$$W_{(KER,KUM,VAN)} = \begin{cases} 0, W_{BB} = 0 \quad OR \quad W_{NM} = 0, \quad OR \quad W_{KDP} = 0 \\ W_{att} + W_{wr} + W_{range} + W_{vel} + W_{CSR}, else \end{cases} \tag{2.1}$$

$$Z_{composite} = \frac{W_{KER} \times Z_{KER} + W_{KUM} \times Z_{KUM} + W_{VAN} \times Z_{VAN}}{W_{KER} + W_{KUM} + W_{VAN}} \tag{2.2}$$

The initial steps are as follows:

1. The Removal of non-meteorological targets (W_{NM}) by utilizing the weather echo classification from each radar. The weather echo class is determined by a fuzzy logic algorithm which utilizes the dual-polarimetric parameters to classify the echoes (Keräinen et al 2014).
2. Absolute calibration of Z_H using the self-consistency between Zh and Φ_{dp} for rain (Gorgucci et al. 1992; Goddard et al 1994), and follows the procedures presented by Gourley et al. (2009).

With these steps accomplished, a set of weights are calculated for each radar. Beam blockage from buildings and trees was determined for the radars by utilising laser scanning data fro the National Land Survey of Finland, providing an accurate elevation of elevation of the objects in the radar's horizon. A beam was classified as suffering form partial beam blockage by using a 3 dB Gaussian beam shape which is a ratio of the unblocked and blocked total power. A beam is considered free from beam blockage when the ratio is less than 1 dB. Beams with no beam blockage have a weight (W_{BB}) equal to 1, else equal to 0. Ground clutter is accounted for with two weights: W_{VEl} and W_{CSR}. All radars undergo a Doppler ground clutter filter, the Gaussian model adaptive processing or GMAP (Siggia and Passarelli 2004). Signal loss when velocities of precipitation are close to zero and some ground clutter can escape the filter. W_{vel} was created to account for this signal loss. When the mean velocity normalized by the unambiguous velocity is less than 0.1, indicating ground clutter, W_{vel} is set to 0.01, and greater than 0.1 receives the full weight. Though K_{dp} is typically immune to clutter, there appeared an unknown error at the edges of W_{vel} field, while the source of this uncertainty is known it was accounted for in the K_{DP} composite. An additional clutter filter was created using the clutter-to-signal ratio (W_{CSR}) for residual clutter. Echoes where the CSR was greater than 25 dB was determined as classified as clutter and the W_{CSR} was set to 0.01, and when CSR was less than 20 the echo received the full weight. Values in between followed the following, $W_{CSR} = (25 + CSR_{obs}) / (25\text{-}20)$.

Two forms of attenuation were accounted for: path attenuation and wet radome attenuation. Path attenuation was determined on a ray by ray case. A linear relationship between Z_H loss and Φ_{dp} (Ryzhkov and Zrnić 1995) was used to determine the attenuation as following : $0.0688 \times \Phi_{dp}$ (Carey et al 2000). The maximum allowed attenuation as set to 3 dB (Watt=0.01), and the minimum qualifying as attenuation was set to 1 dB (W_{att}=1). Between these values, W_{att} was calculated as W_{att}=3-A_{obs}/(3-1). Wet radome attenuation, when a radar's radome is covered in water leading to signal loss at the radar site, was determined by utilizing Z_H from the other radars above the radar in question. A third degree polynomial, in the form $A_{wr} = -0.001566 \times Z_H^2 - 0.01516 \times Z_H + 0.03765$, was found to represent the loss of Z_H well. W_{WR} was set to 0. 01, when the A_{wr} was greater than 3dB, and 1 when A_{wr} was less than 1. Between 1 and 3, the $W_{WR} = (3\text{-}A_{wr})/(3\text{-}1)$.

The correction for overshooting and echo height discrepancies due to differing elevation angles was taken into account with W_{range}. As the radars can operate at different elevation angles, and even equal distance echoes can represent different heights. To correct for this, the height of the echo was used, calculated form by utilizing the 4/3 earth model. An adapted calculation for the W_{range} from Zhang et al (2005) was used to create a less steep gradient. This is due to the relatively close ranges of the radars to one another. W_{range} was calculated is seen in (2.3)

$$W_{range} = \begin{cases} 1, R < R_{min} \\ exp(-\frac{H^2}{2H_{max}^2}) + H_{min}, R \geqslant R_{min} \end{cases} \tag{2.3}$$

where H_{max} is 2 km, and H_{min} is the height of the beam at 0.3 km. Near radar echoes (range<0.3km) is set to 1 to utilize the nearest radar.

K_{DP} required an additional filter to remove spurious results. A self-consistency filter (W_{KDP}) was applied to correct remove these. This utilized the relationship defined in Gourley et al (2009), and removed values values that varied more than $\pm 10^{-3}$ ° km^{-1}. Values outside this range received a weight of 0, and inside received the full weight of 1.

2.2. Quantitative Precipitation Estimation and interpolation of Precipitation

Utilising the composited Z_H and K_{dp} fields, the rain rate was computed using the formulations found specifically fro five years of disdrometer data in Finland from Leinonen et al. (2012), and the relationships can be found therein. A blended QPE decision method was used to created to take into account the strengths and weaknesses of K_{dp} and Z_H and to increase the accuracy and reliability of the QPE (Giangrande and Ryzhkov 2008). R(ZH) was used for light rain and drizzle, where the rain rate was less than 4 m/s. R(K_{DP}) was used for possible hail cases, defined here when Z_H was above 50 dBZ, and heavy rain, when Z_H was greater than 20 dBZ and K_{dp} was greater than 0.1 ° km^{-1}.

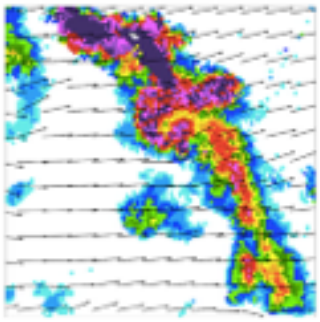

Figure XXX: Motion vectors of precipitation estimate. Black arrows show direction of motion.

Interpolation was performed on the precipitation fields to increase the number of observations, from every five minutes to 1 minute. An example of the calculated motion fields is seen in Figure XXX. Interpolation was performed by calculating the motion vectors based on the optic flow algorithm, which utilizes the changing position of objects to recognise motion. We used a python packaged Optflow (Pulkinnen 2016) for the interpolation process.

3. Results

3.1. Composite

Compositing was performed for the summer months of 2016. Events were chosen based on the presence of precipitation and the lack of a bright band, which would require additional quality control steps. An example of corrected and composited Z_H and K_{DP} can seen in Figure 3.

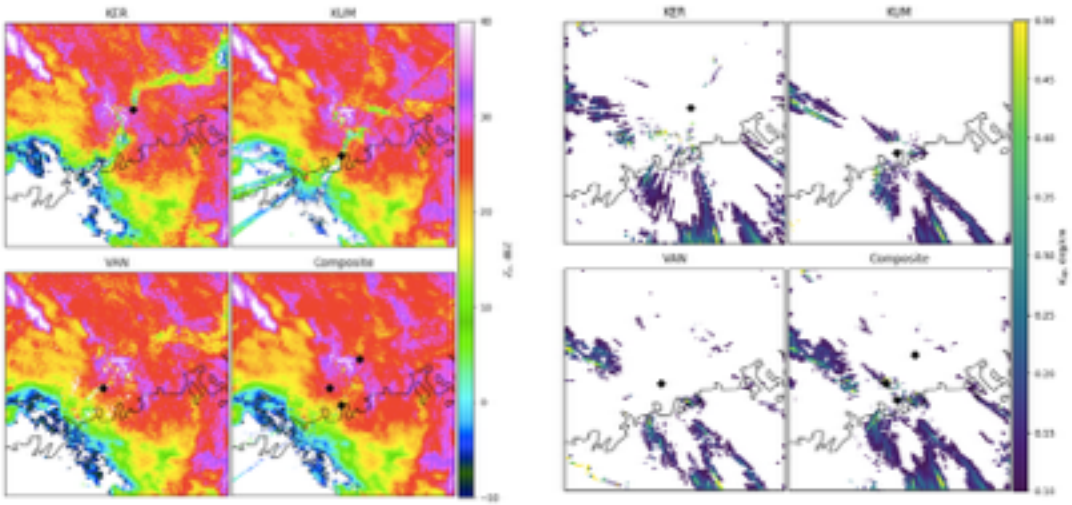

Figure 3: Reflectivity (left) and Specific differential phase (right) for two separate events. KER, KUM, VAN, and the composite are shown. Note low Kdp (<0.1° km^{-1}) have been removed.

Figure 3 shows the Zh and Kdp for KER, KUM, VAN and the composite. Large improvements can be seen in the composited Z_H over individual scans. The effect of W_{vel} , can be seen in all three radars, seen as a zone of decreased Z_H

snaking out from the radar. In the composite this error is removed and realistic Z_H are shown. Path attenuation is taken in all radars, but can be seen especially in KUM towards the east. This is corrected in the composite with higher Z_H. All three radars are being rained on eat this moment. However the reflectivity above KUM is the lowest and falls below the minimum A value (1dB) and receive the full W_{wr} weight, as opposed to the other two which are reduced. a KUM also suffers from 2nd trip echoes; these are removed/weakened with the combination of the other radars. However the composite does include weakened 2nd trip echoes that were not present in the other radars. So some sleight errors, including some speckle, are transferred to the composite. The K_{dp} composite shows how the K_{dp} can be blended. Large values of K_{DP} seen in the south west in KUM and VAN are removed in the composite. This is due to the W_{KDP} filter removing spurious values.

3.2. QPE

Composite was verified with a gauge comparison of rain rates from the summer 2017. Five rain gauges fall within the composite area used. Two of these gauges are in the city, one of which is located in at the KUM radar location, and another in the city center (Kaisaniemi). Figure 4 shows the gauge comparison for the Kaisaniemi gauge, and all five gauges combined for the FMI VAN radar, and the composite.

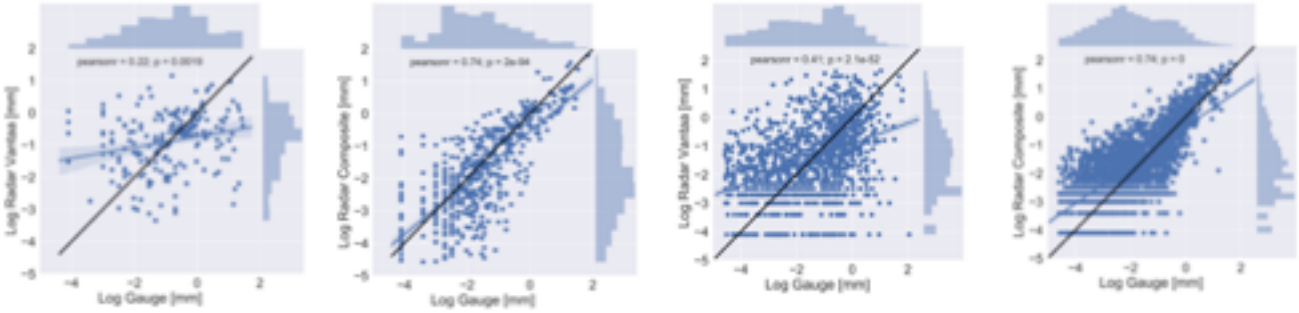

Figure 4: Radar to gauge comparisons for the FMI VAN radar at the Kaisaniemi gauge (A) and all gauge (B), and radar to gauge comparison for the composite Kaisaniemi gauge (C) and all gauges (D). All plots are in log-log format. Black line indicates the 1-1 relationship, and a linear fit is shown as a blue line in each plot. The distribution for all gauges and radar are seen in the margins.

The comparison for the Kaisaniemi gauge and the VAN radar and composite is clear. The composite greatly outperforms the VAN radar for city precipitation estimation in the city center. VAN suffers from considerable echo removal due to clutter suppression techniques. The composite is able to correct for this. The composite also overestimates all low rain rates. This is possibly due to the interpolation adding additional observations. The gauges are 10 minute averages accumulations. Therefore in very low precipitation rates the radar may out perform the gauges. The composite also shows improvement over VAN for all gauges, however to a lesser degree. The bias, standard deviation, and root mean square error can be seen in Table 1. The table shows that the composite outperforms VAN alone.

Table 1:Mean biases, standard deviations, and root mean square error for the composite and VAN radar for both Kaisaniemi and all gauges (including Kaisaniemi).

	Bias [mm]	SD [mm]	RMSE [mm]
Composite Kaisaniemi	-0.07	0.08	0.28
VAN Kaisaniemi	3	0.48	0.70
Composite All Guages	-0.05	0.09	0.30
VAN All Guages	-0.1	0.49	0.70

Finally, Figure 5 shows the VAN radar and composite 24 hour accumulation for a single day in 16.06.2016. The effect of VAN's clutter suppression is highly visible in the accumulation. This leaves large gaps over the city, located to the south east of VAN (black dot)

3. Discussion

In order to produce the highest quality precipitation estimate over the city of Helsinki in Finland and quality controlled composite was created from three C band radars. A series of quality controlled weights and an absolute calibration of the three radars were implemented to create the highest quality data. The composited data was then used to create a precipitation estimate. A blended precipitation rate was created with $R(Z_H)$ and $R(K_{DP})$ to increase the reliability of the measurements.

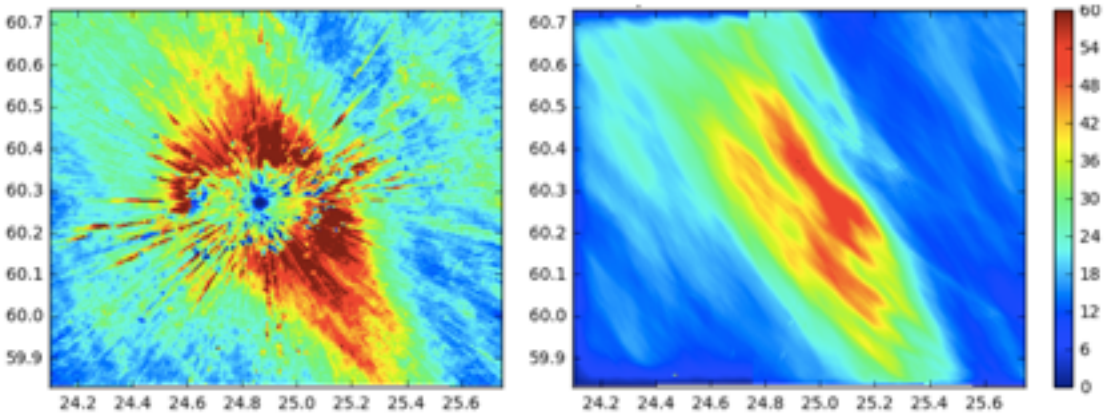

Figure 5 VAN (right) and composite (left) 24 hour precipitation accumulation fro 16.06.2016.

By utilising five gauges within the Helsinki region to compare the rain rate estimate to surface observations a significant improvement can be seen between the FMI VAN radar, which is part of the Finnish national radar grid, and the Helsinki composite, and errors are reduced for composite. However, errors can be transferred from individual radars to the composite. The most prominent errors consist of 2nd trip echoes, and speckle.

Acknowledgement

I would like to than AnnaKaisa von Lerber for her help in providing all the vantaa radar data and gauge data.

References

Berne, A. Delrieu, G. Creutin, J. and Obled, C. 2004: Temporal and spatial resolution of rain- fall measurements required for urban hydrology. *Journal of Hydrology*, 299 (3-4), 166–179,

Carey, L. Rutledge, S. Ahijevych, D. and Keenan, T. 2000: Correcting propagation effects in c-band polarimetric radar observations of tropical convection using differential propagation phase. *Journal of Applied Meteorology*, 39 (9), 1405–1433.

Einfalt, T. Arnbjerg-Nielsen, K. Golz, C. Jensen, N. Quirmbach, M. Vaes, G. and Vieux, B. 2004: Towards a roadmap for use of radar rainfall data in urban drainage. *Journal of Hydrology*, 299 (34), 186 – 202

Friedrich, K. Hagen, M. and Einfalt, T. 2006: A quality control concept for radar reflectivity, polarimetric parameters, and doppler velocity. *Journal of Atmospheric and Oceanic Technology*, 23 (7), 865–887,

Giangrande, S. and Ryzhkov, A. 2008: Estimation of rainfall based on the results of polarimetric echo classification. *Journal of Applied Meteorology and Climatology*, 47 (9), 2445–2462

Goddard, J. Tan, , J. and Thurai, M. 1994: Technique for calibration of meteorological radars using differential phase. *Electronics Letters*, 30 (2), 166–167.

Gorgucci, E. Bechini, R. Baldini, L. Cremonini, R. and Chandrasekar, V. 2013: The influence of antenna radome on weather radar calibration and its real-time assessment. *Journal of Atmospheric and Oceanic Technology*, 30 (4), 676–689

Gourley, J. Illingworth, A. and Tabary, P. 2009: Absolute calibration of radar reflectivity using redundancy of the polarization observations and implied constraints on drop shapes. *Journal of Atmospheric and Oceanic Technology*, 26 (4), 689–703

Leinonen, J. Moisseev, , D. Leskinen, M. and Petersen, W. 2012: A climatology of disdrometer measurements of rainfall in Finland over five years with implications for global radar observations. *Journal of Applied Meteorology and Climatology*, 51 (2), 392–404

Pulkinnen, S. 2016: C++/Python implementations of optical flow algorithms. https://github.com/pulkkins/Optflow, Url visited on 21.06.2018

Ryzhkov, A. and Zrnic´, D. 1995: Comparison of dual-polarization radar estimators of rain. *Journal of Atmospheric and Oceanic Technology*, 12 (2), 249–256

Saltikoff, E. Huuskonen, A. ,Hohti, H. , Koistinen, J. and J. Heikki, 2010: Quality assurance in the FMI doppler weather radar network. *Boreal environment research*, 15 (6), 579–594.

Siggia, A. and Passarelli, J. 2004: Gaussian model adaptive processing (gmap) for improved ground clutter cancellation and moment calculation, Visby, Sweden. ERAD, 67–73, [Available online at http://copernicus.org/erad/2004/online/ERAD04 P 67.pdf.].